Simulation of fully developed laminar free convection flow between vertical parallel flat plates

Simulación de flujo laminar de convección libre completamente desarrollado entre placas planas paralelas verticales

Simulação de escoamento laminar de convecção livre totalmente desenvolvido entre placas planas verticais paralelas

Héctor Espinoza-Roman [1] [(*)]

Recibido: 18/02/2026 Aceptado: 14/04/2026

Summary. - This study presents a numerical investigation of laminar free convection between vertical parallel plates with asymmetric uniform wall temperatures. The right wall is maintained at a higher temperature than the left. Fluid enters the channel at a temperature less than or equal to the cooler wall. Using the finite volume method in OpenFOAM v13, the governing equations are solved and validated against classical analytical solutions. A systematic grid convergence study ensures spatial independence. Results show that while the linear temperature profile is accurately captured on coarse grids, the cubic velocity profile requires higher resolution for precision. The findings validate the numerical methodology and offer critical insights into mesh requirements for accurately simulating fully developed natural convection flows in vertical channels.

Keywords: *heat transfer; passive ventilation; solar chimney; CFD.*

(*) Corresponding author.
[1] Mechanical Engineer, MSc in Computational Mechanics, PhD in Engineering, Dirección de Investigación e Innovación, Fundación Universitaria Antonio de Arévalo UNITECNAR (Colombia); hector.espinoza@unitecnar.edu.co; ORCID iD: https://orcid.org/0000-0002-2861-2442

Memoria Investigaciones en Ingeniería, núm. 30 (2026). pp. 244-255
https://doi.org/10.36561/ING.30.16
ISSN 2301-1092 • ISSN (en línea) 2301-1106 – Universidad de Montevideo, Uruguay

Resumen. - *Este estudio presenta una investigación numérica de la convección libre laminar entre placas verticales paralelas con temperaturas de pared uniformes y asimétricas. La pared derecha se mantiene a una temperatura más alta que la izquierda. El fluido entra al canal a una temperatura menor o igual a la de la pared más fría. Utilizando el método de volúmenes finitos en OpenFOAM v13, se resuelven las ecuaciones que rigen el proceso y se validan frente a soluciones analíticas clásicas. Un estudio sistemático de convergencia de mallas garantiza la independencia espacial. Los resultados muestran que, si bien el perfil de temperatura lineal se captura con precisión en mallas gruesas, el perfil de velocidad cúbico requiere una mayor resolución para mayor precisión. Los hallazgos validan la metodología numérica y ofrecen información crucial sobre los requisitos de la malla para simular con precisión flujos de convección natural completamente desarrollados en canales verticales.*

Palabras clave: *transferencia de calor; ventilación pasiva; chimenea solar; CFD.*

Resumo. ***-*** *Este estudo apresenta uma investigação numérica da convecção livre laminar entre placas verticais paralelas com temperaturas de parede uniformes e assimétricas. A parede direita é mantida a uma temperatura mais alta que a esquerda. O fluido entra no canal a uma temperatura menor ou igual à da parede mais fria. Utilizando o método de volumes finitos no OpenFOAM v13, as equações que governam o processo são resolvidas e validadas em comparação com soluções analíticas clássicas. Um estudo sistemático de convergência da malha garante a independência espacial. Os resultados mostram que, embora o perfil linear de temperatura seja capturado com precisão em malhas grosseiras, o perfil cúbico de velocidade requer maior resolução para maior precisão. As descobertas validam a metodologia numérica e fornecem informações cruciais sobre os requisitos de malha para simular com precisão fluxos de convecção natural totalmente desenvolvidos em canais verticais.*

Palavras-chave: *Transferência de calor; ventilação passiva; chaminé solar; CFD.*

1. Introduction. - The motivation of this article is to serve as a starting point for the simulation of solar chimneys. Free convection is the driving force that generates flow in a solar chimney. The steady-state, fully developed laminar free convection between parallel flat plates is one of the most basic cases of free convection. Additionally, it has an analytical solution, which allows for a direct comparison and validation of simulation results in terms of velocity, temperature, pressure, and flow rate.

Solar chimneys, as a passive and sustainable ventilation and energy generation technology, have been the subject of extensive recent research. Contemporary studies have focused on optimizing their complex geometries, including roof-mounted configurations [1, 2, 3], high-rise designs for uniform flow [4, 5], and folded or curved façades [6, 7]. The performance of these systems under various climatic conditions and integration with other building components, such as earth-to-air heat exchangers [8] or within specific building types like aged-care centers [9] and urban tunnels [10], has been rigorously investigated. Furthermore, comprehensive reviews by [11] and [12] underscore the maturity of the field while highlighting the persistent reliance on Computational Fluid Dynamics (CFD) as a primary investigative tool.

The accuracy of any CFD simulation for such applications, however, is fundamentally dependent on the proper resolution of the buoyancy-driven flow physics at its core. Before tackling the geometrical and turbulent complexities of real-world solar chimneys, it is imperative to ensure that the numerical methodology can precisely reproduce the underlying convective phenomena. The canonical case of laminar free convection between vertical, asymmetrically heated parallel plates serves as a critical benchmark for this purpose [13, 14, 15, 16, 17, 18]. This flow configuration is not only representative of the core physics in a solar chimney's flow channel but also possesses a well-established analytical solution [13, 14] providing an unambiguous standard for code verification.

While Direct Numerical Simulation (DNS) studies of turbulent flows in similar configurations exist [19], and several authors have employed CFD for performance analysis [20, 21], a clear gap remains in the literature regarding the meticulous verification of the numerical schemes and mesh requirements specifically for the laminar case using open-source CFD software OpenFOAM. Many studies proceed directly to complex applications without first demonstrating that their solver can accurately capture the basic velocity and temperature profiles that form the building blocks of the flow. This step is crucial for gaining confidence in simulation results, as errors introduced at this fundamental level can propagate and be amplified in more complex cases.

Therefore, this study aims to bridge this gap by presenting a detailed numerical investigation of the thermally developed, laminar free convection between vertical parallel plates with asymmetric uniform wall temperatures. Using the open-source CFD toolbox OpenFOAM, we systematically perform a grid convergence study to establish the mesh independence of the results. The primary objective is to validate the numerical methodology by demonstrating its ability to asymptotically approach the classical analytical solutions for both the temperature and velocity profiles in the fully developed regime. By doing so, this work provides a verified foundation upon which more complex simulations of solar chimneys and other natural convection applications can be reliably built.

2. Problem statement. - This section details the equations that govern the laminar free convection between vertical parallel plates as well as the boundary conditions and nondimensionalization of equations and variables.

2.1 Governing Equations. - The flow is assumed to be two-dimensional, steady, incompressible and laminar. The Boussinesq approximation is adopted to model the buoyancy force, whereby density variations are considered only in the body force term of the momentum equation. Under these assumptions, the governing equations for conservation of mass, momentum, and energy are given by:

$$\nabla \cdot \mathbf{u} = 0, \tag{1}$$

$$\mathbf{u} \cdot \nabla \mathbf{u} + \frac{1}{\rho} \nabla p - \nu \Delta \mathbf{u} = \beta (T - T_0) \mathbf{g}, \tag{2}$$

$$\mathbf{u} \cdot \nabla T - \alpha \Delta T = 0, \tag{3}$$

where u is the velocity vector, p is the pressure, T is the temperature, g is the gravitational acceleration vector, ρ is the reference density, ν is the kinematic viscosity, $\alpha = k/(\rho c)$ is the thermal diffusivity, β is the thermal expansion coefficient and T_0 is the reference temperature.

2.2 Dimensionless Governing Equations. - The dimensionless governing equations [13, 14], taking into account that $U = 0, V(X)$ and $\theta(X)$ are:

$$\frac{\mathrm{d}P}{\mathrm{d}X} = 0, \tag{4}$$

$$\frac{\mathrm{d}P}{\mathrm{d}Y} - \frac{\mathrm{d}^2V}{\mathrm{d}X^2} = \theta, \tag{5}$$

$$-\frac{\mathrm{d}^2\theta}{\mathrm{d}X^2} = 0, \tag{6}$$

where,

$$X = \frac{x}{b}, \quad Y = \frac{y}{l\mathrm{Gr}}, \tag{7}$$

$$U = \frac{bu}{\nu}, \quad V = \frac{b^2v}{l\nu\mathrm{Gr}}, \tag{8}$$

$$P = \frac{(p-p_0)b^4}{\rho l^2\nu^2\mathrm{Gr}^2}, \quad \theta = \frac{T-T_0}{T_1-T_0}, \tag{9}$$

$$\mathrm{Pr} = \frac{\mu c}{k}, \quad \mathrm{Gr} = \frac{g\beta(T_1-T_0)b^4}{l\nu^2}. \tag{10}$$

The temperature difference ratio r_T is defined as:

$$r_T = \frac{T_2-T_0}{T_1-T_0}, \tag{11}$$

whereas the dimensionless flow rate is:

$$M = \frac{u_0b^2}{l\nu\mathrm{Gr}}. \tag{12}$$

2.3 Dimensionless Exact Solution. - The exact solution [13, 14] for dimensionless velocity, pressure and temperature is:

$$U = 0, \tag{13}$$

$$V = (r_T-1)\frac{X^3}{6} - r_T\frac{X^2}{2} + (2r_T+1)\frac{X}{6}, \tag{14}$$

$$P = 0, \tag{15}$$

$$\theta = (1-r_T)X + r_T. \tag{16}$$

The volumetric flow rate M is:

$$M = \frac{r_T+1}{24}. \tag{17}$$

The dimensionless average velocity U_0 can be calculated as:

$$U_0 = M. \tag{18}$$

It happens that M and U_0 are numerically equal, but they refer to different magnitudes. M is a volumetric flow rate whereas U_0 is the average velocity.

The dimensionless coordinate of the maximum velocity is:

$$X_{\max} = \frac{2r_T + 1}{3r_T + A}, \tag{19}$$

where $A = \sqrt{3(r_T^2 + r_T + 1)}$.

The dimensionless maximum velocity is:

$$U_{\max} = \frac{X_{\max}}{18}\left[3(2r_T + 1) - (6r_T + A)X_{\max}\right]. \tag{20}$$

2.4 Domain and Boundary Conditions. - The domain is a two-dimensional vertical channel of height L and gap width b, as illustrated in Figure I.

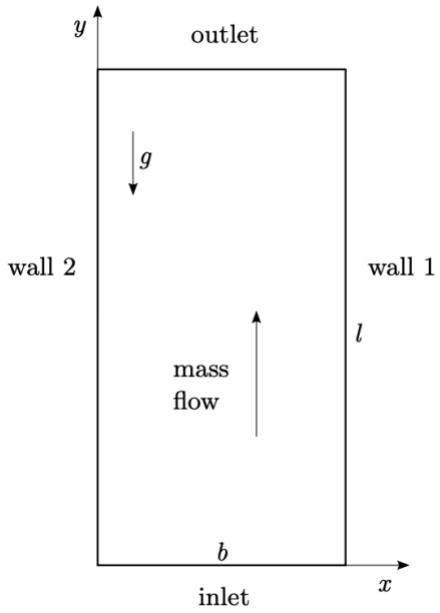

Figure I. Schematic of the domain and boundary conditions.

The following boundary conditions are applied:

- Right Wall (hot): No-slip velocity condition $u = 0$ and uniform wall temperature $T = T_1$.
- Left Wall (cold): No-slip velocity condition $u = 0$ and uniform wall temperature $T = T_2$.
- Inlet (bottom): uniform pressure $p = 0$ and linear temperature variation $T(x = 0) = T_2$ and $T(x = b) = T_1$.
- Outlet (top): uniform pressure $p = 0$ with zero-gradient for velocity and temperature.

The average temperature is defined as:

$$\overline{T} = \frac{T_1 + T_2}{2}, \tag{21}$$

and the average temperature difference is:

$$\overline{\Delta T} = \overline{T} - T_0. \tag{22}$$

2.5 Fluid properties, domain size and boundary values. - The values used for the simulation are for air at atmospheric pressure and temperature of 30 C. The values are summarized in Table I.

Magnitude	Value	Derived Magnitude	Value
g	9.8 m/s^2	$\overline{T}$	40 °C
T_0	30 °C	ν	1.608E-5 m^2/s
T_1	42.5 °C	k	0.02588 W/(m K)
T_2	37.5 °C	α	2.208E-5 m^2/s
b	0.005 m	Gr	0.6512
l	1.5 m	r_T	0.6
ρ	1.164 kg/m^3	$\overline{\Delta T}$	10 °C
β	3.299E-3 1/K	-	-
c	1007 J/(kg K)	-	-
μ	1.872E-5 Pa s	-	-
Pr	0.7282	-	-

Table I. Values of magnitudes and derived magnitudes.

3. Numerical simulation procedure. - The open-source Computational Fluid Dynamics (CFD) toolbox OpenFOAM (version v13) was used to solve the governing equations (1)–(3). The steady-state solver fluid, which implements the SIMPLE (Semi-Implicit Method for PressureLinked Equations) algorithm for pressure-velocity coupling, was employed. The solver was configured with laminar simulation type. The Boussinesq approximation was used as equation of state.

The spatial discretization schemes were first-order accurate. The Gauss linear scheme was used for the gradient terms, the bounded Gauss upwind scheme was used for the divergence terms, and the Gauss linear corrected scheme was used for the Laplacian terms. An under-relaxation factor of 0.8 was applied to ensure numerical stability during the iterative solution process. Simulations were considered converged when the normalized residuals for all variables fell below 10−8. More details of the exact set up can be seen in the OpenFOAM case file. Very stable schemes were used in order to avoid instabilities due to the thermally driven flow in the first iterations.

3.1 Mesh Independence Study. - A systematic grid convergence study was conducted to ensure that the numerical results were independent of the mesh resolution. Three sequentially refined structured meshes were generated, characterized by an increasing number of cells in the transverse direction to better resolve the fluid field. All meshes have uniform grading. The details of these meshes are provided in Table II.

Mesh	Number of Cells ($N_x \times N_y$)	Total Cells
Mesh04	4×100	400
Mesh08	8×100	800
Mesh15	15×100	1,500
Mesh16	16×100	1,600
Mesh32	32×100	3,200
Mesh64	64×100	6,400

Table II. Details of the meshes used for the grid convergence study.

4. Results and discussion. - This section presents and discusses the numerical results obtained from the simulations of fully developed laminar free convection flow in a vertical channel. The primary objective is to validate the computational methodology by comparing the predicted temperature and velocity profiles against the analytical solution. The influence of mesh resolution on the accuracy of these profiles is examined in detail.

Figure II shows the temperature along the centerline ($X = 0.5$) from the inlet ($y = 0$) up to the outlet ($y = l$) for Mesh16. It can be seen that for 80% of the channel height ($y = 1.2$) the flow is thermally developed and there is no interference from the outlet boundary.

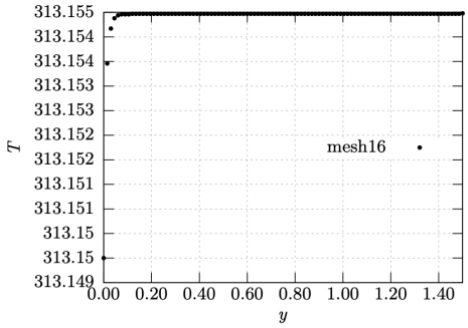

Figure II. Temperature along the centerline of the channel.

Figure III shows the y-velocity (v) along the centerline ($X = 0.5$) from the inlet ($y = 0$) up to the outlet ($y = l$) for Mesh16. It can be seen that for 80% of the channel height ($y = 1.2$) the flow is hydrodynamically developed and there is no interference from the outlet boundary.

Therefore, the fully developed profiles were measured at 80% of channel height l in order to be sufficiently downstream of the flow and to have a reasonable separation from the outlet boundary.

4.1 Temperature Profile. - Figure IV shows the dimensionless temperature profile, θ, across the channel width for the three meshes alongside the analytical solution. As anticipated by the linear form of the analytical solution for the temperature field in the fully developed region, the numerical method reproduces it with exceptional accuracy across all mesh resolutions, including the coarsest mesh. The profiles are visually indistinguishable from the analytical line.

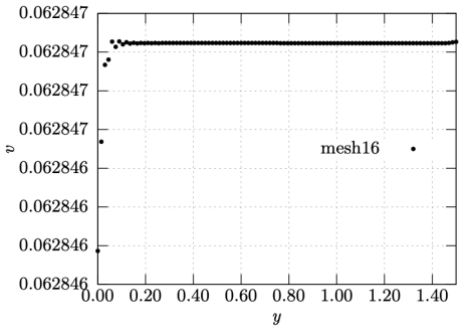

Figure III. y-velocity along the centerline of the channel.

The correct imposition of the Dirichlet boundary conditions is confirmed by the data points at the walls; the dimensionless temperature at the left wall ($X = 0$) is θ = 0.0 and at the right wall ($X = 1$) is $\theta = 1.0$, exactly as specified. This perfect agreement is expected for a linear profile, as it can be exactly captured by the linear shape functions of the finite volume method, even with a minimal number of cells. This result serves as a primary check, verifying that the thermal boundary conditions and the energy equation discretization have been imposed correctly.

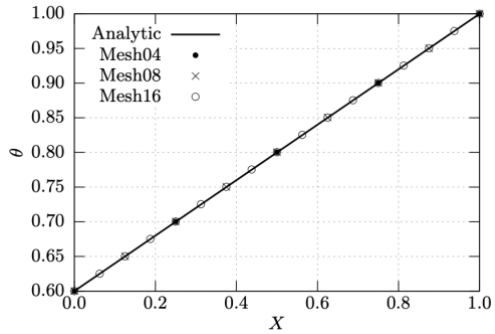

Figure IV. Temperature profile.

4.2 Velocity Profile. - The validation of the velocity field presents a more stringent test for the numerical method. Figure V displays the dimensionless vertical velocity profile, V, for the three meshes compared to the analytical solution. Velocity was extracted from the mesh by sampling using an interpolation scheme cellPoint of type lineFace.

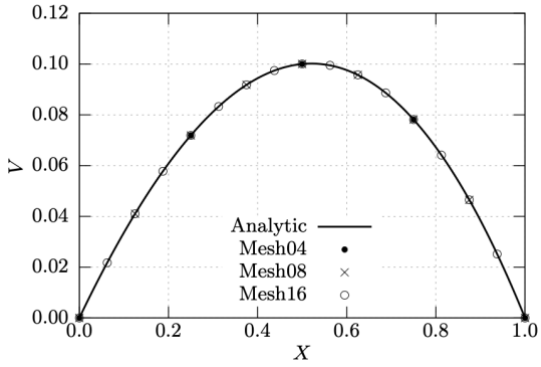

Figure V. Vertical velocity profile.

The no-slip boundary condition is correctly satisfied on both walls ($X = 0, V = 0$ and $X = 1, V = 0$) for all meshes. The location and value of the maximum velocity near the channel centerline ($X \approx 0.5$) are also captured remarkably well, even on the coarsest mesh.

In order to see the velocity profile by cell values, velocity is plotted in Figure VI. Velocity was extracted from the mesh by sampling using an interpolation scheme cell of type lineCell. This just takes the cell values (velocity and coordinate) without interpolation. In this figure, the differences between meshes can be seen more clearly: coarsest mesh produces the less accurate result, and the finest mesh produces the most accurate result as expected. Notably, even the coarsest mesh (Mesh04) demonstrates a high degree of fidelity, providing a close approximation of the analytical solution.

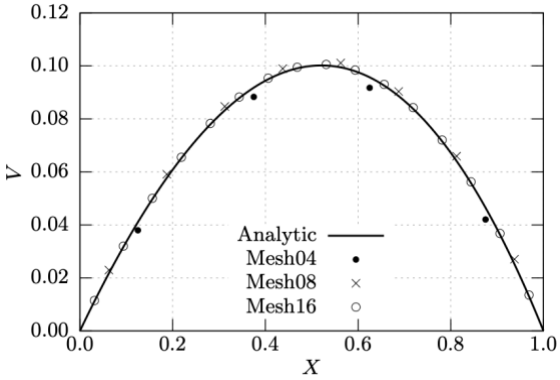

Figure VI. Vertical velocity profile (cell).

4.3 Pressure Profile. - Figure VII displays the dimensionless pressure profile, P, for the three meshes compared to the analytical solution. Pressure is correctly captured by all the meshes.

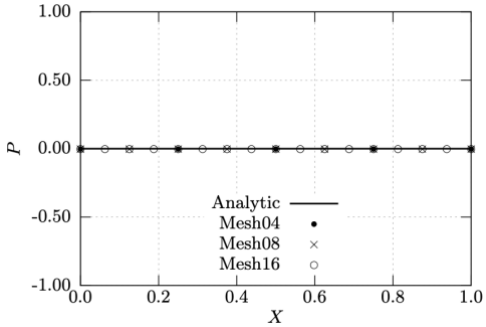

Figure VII. Pressure profile.

4.4 Quantitative Error Analysis. - To move beyond a visual comparison, a quantitative analysis of the discretization error was performed. The relative error in the maximum velocity (ϵ_{Vmax}) and the relative error in the position of the maximum velocity (ϵ_{Xmax}) were calculated for each mesh relative to the analytical solution. The values for each mesh were extracted using cellPoint interpolation with lineFace sampling. The results are summarized in Table III. It can be seen that the error in the maximum velocity is already very small in the coarse mesh and there is, apparently, very little improvement in the finer meshes. The error in the position of the maximum velocity as well stays constant. This is an artifact due to the sampling type lineFace used because Mesh04 to Mesh16 do not capture the maximum velocity position well for that sampling method. We have to point out that, for this case, the exact velocity profile is not symmetric, and the maximum velocity is reached at $X = 0.5207$. However, the meshes we are using do not capture that point closely. To overcome that, a mesh with 15 divisions is added to the table and it shows better agreement with the maximum velocity value and position value. However, another comparison is done using another sampling type and shown in the next table.

Mesh	$X_{\max}$	$\epsilon_{X_{\max}}$ (%)	$V_{\max}$	$\epsilon_{V_{\max}}$ (%)
Mesh04	0.5000	-3.98	0.1000249	0.15
Mesh08	0.5000	-3.98	0.1000257	0.15
Mesh16	0.5000	-3.98	0.1000259	0.15
Mesh15	0.5333	2.42	0.1001343	0.04
Analytical	**0.5207**	–	**0.1001730**	–

Table III. Quantitative error analysis for the maximum vertical velocity.

Now, in order to compare quantitatively the cell velocity extracted using an interpolation scheme cell and sampling type lineCell, Table IV shows the error in the maximum cell velocity value and position. It can be seen the convergence in the maximum velocity position as well as the convergence on the maximum velocity value.

Let us now compare the dimensionless volumetric flow rate M. Flow rate is a key magnitude to have into account when analyzing solar chimneys for ventilation. Table V shows the volumetric flow rate and its error for various meshes. It can be seen the monotonous convergence of M when refining the mesh.

Mesh	$X_{\max}$	$\epsilon_{X_{\max}}$ (%)	$V_{\max}$	$\epsilon_{V_{\max}}$ (%)
Mesh04	0.62500	20.0	0.0917403	-8.42
Mesh08	0.56250	8.02	0.1010997	0.92
Mesh16	0.53125	2.02	0.1005507	0.38
Analytical	**0.52072**	–	**0.1001730**	–

Table IV. Quantitative error analysis for the maximum vertical velocity (cell).

Mesh	M	ϵ_M (%)
Mesh04	0.0750164	12.5
Mesh08	0.0687656	3.15
Mesh16	0.0672029	0.80
Mesh32	0.0668121	0.22
Mesh64	0.0667140	0.07
Analytical	**0.0666667**	–

Table V. Quantitative error analysis for volumetric flow rate.

Let us focus now on mass flow rate. Table VI shows the mass flow rate for various meshes. The dimensional mass flow rate ($\dot{m}$) was computed taking the depth of the channel equal to its width. The dimensionless numerical mass flow rate was computed by first converting the mass flow rate to volumetric flow rate using density at $\bar{T}$ and then nondimensionalizing this value. The exact dimensionless mass flow rate was taken equal to the dimensionless volumetric flow rate.

Mesh	$\dot{m}$ (kg/s)	$\dot{M}$	$\epsilon_{\dot{M}}$ (%)
Mesh04	1.3260E-6	0.0750011	12.5
Mesh08	1.2156E-6	0.0687545	3.13
Mesh16	1.1880E-6	0.0671930	0.79
Mesh32	1.1811E-6	0.0668025	0.20
Mesh64	1.1793E-6	0.0667045	0.06
Analytical	**1.1794E-6**	**0.0666667**	–

Table VI. Quantitative error analysis for mass flow.

As can be seen in the tables of the quantitative error analysis, even with low order schemes, a good convergence is obtained. So, it was decided that there is no need to go for higher order schemes.

5. Conclusion. - This study has successfully conducted a detailed numerical verification of laminar free convection in a vertical channel with asymmetric wall temperatures, serving as a foundational benchmark for simulating more complex systems like solar chimneys. The key findings and implications of this work are summarized as follows:

a. Successful Methodology Validation: The implemented model in OpenFOAM v13 has demonstrated a robust capability for simulating buoyancy-driven flows. The numerical solutions showed excellent agreement with the analytical profiles for the fully developed region, thereby validating the chosen computational approach and the implementation of the physical models.

b. Critical Role of Mesh Resolution: A systematic grid convergence study revealed a distinct sensitivity to mesh density based on the flow variable of interest. The linear temperature profile, characteristic of the fully developed thermal field, was accurately reproduced even on relatively coarse meshes. In contrast, the cubic velocity profile, required progressively finer meshes to be captured with high fidelity. Remarkably, the model captures the velocity profile very well even for the coarsest mesh. This underscores the importance of a mesh-independent study and indicates that the velocity field is the more critical metric for determining sufficient spatial resolution in this type of simulation.

c. Practical Implications for Solar Chimney Simulation: The findings provide a crucial practical guideline for CFD modeling of solar chimneys and similar passive ventilation systems. While simplified models might adequately predict temperature distributions, accurate prediction of airflow rates, which is directly tied to the velocity profile, requires a certain grid resolution. This insight is essential for optimizing computational resources without sacrificing the accuracy of key performance metrics, such as ventilation flow rate.

d. Foundation for Future Work: This rigorously verified setup forms a reliable foundation for subsequent research. The validated methodology can be confidently extended to investigate more complex and realistic scenarios, including turbulent flow regimes, geometrically complex channels relevant to advanced solar chimney designs and transient solar loading conditions.

In conclusion, this work reaffirms the necessity of fundamental verification as a critical first step in computational fluid dynamics. By establishing a benchmark for accuracy in a canonical case, it enhances the reliability of future numerical studies aimed at optimizing and designing efficient natural convection systems for sustainable building engineering.

References

[1] C. Wang, Y. Wu, C. Hua, X. Zhao, J. Zang, and N. Gao, "Numerical investigation on the influence of geometric parameters on turbulent flow and thermal performance in the roof solar chimney," Building and Environment, vol. 267, p. 112210, 2025.
[2] A. Vazquez-Ruiz, J. M. A. Navarro, J. F. Hinojosa, and J. P. Xamán, "Effect of the solar roof chimney position on heat transfer in a room," International Journal of Mechanical Sciences, vol. 209, p. 106700, 2021.
[3] ——, "Computational fluid dynamics and experimental analysis of the heat transfer in a room with a roof solar chimney," Journal of Thermal Science and Engineering Applications, vol. 14, no. 4, p. 041001, 2022.
[4] J. Gong, L. W. Chew, and P. S. Lee, "Shape optimization of high-rise solar chimneys to improve the uniformity of flowrate distribution," Building and Environment, vol. 243, p. 110650, 2023.
[5] ——, "Theoretical model for high-rise solar chimneys and optimum shape for uniform flowrate distribution," Energy, vol. 298, p. 131358, 2024.
[6] J. Ahmadi, M. Mahdavinejad, and S. Asadi, "Folded double-skin façade (DSF): in-depth evaluation of fold influence on the thermal and flow performance in naturally ventilated channels," International Journal of Sustainable Energy, vol. 41, no. 4, pp. 382–411, 2022.
[7] Y. Huang, Y. Tao, L. Shi, Q. Liu, Y. Wang, J. Tu, Q. Peng, and C. Cao, "Thermal and ventilation performance of a curved double-skin facade model," Energy and Buildings, vol. 268, p. 112202, 2022.
[8] F. Pouranian, H. Akbari, and S. M. Hosseinalipour, "Performance assessment of solar chimney coupled with earth-to-air heat exchanger: A passive alternative for an indoor swimming pool ventilation in hot-arid climate," Applied Energy, vol. 299, p. 117201, 2021.
[9] Q. Wang, G. Zhang, Q. Wu, and L. Shi, "Ventilating aged-care center based on solar chimney: Design and theoretical analysis," Energy and Buildings, vol. 266, p. 112145, 2022.
[10] Y. Huang, X. Liu, L. Shi, B. Dong, and H. Zhong, "Enhancing solar chimney performance in urban tunnels: Investigating the impact factors through experimental and theoretical model analysis," Energy, vol. 282, p. 128329, 2023.
[11] B. Zamora, "A review on solar chimneys: from natural convection fundamentals to thermohydraulic best-performance proposals," Processes, vol. 11, no. 2, p. 386, 2023.
[12] S. P. Melgaard, I. T. Nikolaisson, C. Zhang, H. Johra, and O. K. Larsen, "Double-skin façade simulation with computational fluid dynamics: A review of simulation trends, validation methods and research gaps," Building Simulation, vol. 16, no. 12, pp. 2307–2331, 2023.
[13] W. Aung, L. Fletcher, and V. Sernas, "Developing laminar free convection between vertical flat plates with asymmetric heating," International Journal of Heat and Mass Transfer, vol. 15, no. 11, pp. 2293–2308, 1972.
[14] W. Aung, "Fully developed laminar free convection between vertical plates heated asymmetrically," International Journal of Heat and Mass Transfer, vol. 15, no. 8, pp. 1577–1580, 1972.
[15] W. Aung and G. Worku, "Developing flow and flow reversal in a vertical channel with asymmetric wall temperatures," ASME Journal of Heat Transfer, vol. 108, no. 2, pp. 299–304, 1986.
[16] N. Anand, S. Kim, and L. Fletcher, "The effect of plate spacing on free convection between heated parallel plates," ASME Journal of Heat Transfer, vol. 114, no. 2, pp. 515–518, 1992.
[17] V. Terekhov and A. L. Ekaid, "Laminar natural convection between vertical isothermal heated plates with different temperatures," Journal of Engineering Thermophysics, vol. 20, no. 4, pp. 416–433, 2011.
[18] S. Foroushani, D. Naylor, and J. L. Wright, "Heat transfer correlations for laminar free convection in vertical channels with asymmetrically heated isothermal walls," Heat Transfer Engineering, vol. 41, p. 5, 2020.
[19] J. Pallares, A. Fabregat, and C. Lei, "Direct numerical simulation of the fully developed turbulent free convection flow in an asymmetrically heated vertical channel," International Journal of Thermal Sciences, vol. 191, p. 108352, 2023.
[20] A. H. Radwan and M. M. S. Ahmed, "Improving thermal performance and air flow inside the solar chimney by CFD simulation," MSA Engineering Journal, vol. 2, no. 2, pp. 1245–1277, 2023.
[21] S. Rodriguez Miranda, G. O. Gamboa, M. A. Zamora-Antuñano, N. Farrera-Vázquez, and R. García-García, "CFD evaluation of thermal conditioning in a house of social interest with a solar chimney arrangement in Guanajuato, Mexico," Processes, vol. 11, no. 4, p. 1286, 2023.

Author contribution:
1. Conception and design of the study
2. Data acquisition
3. Data analysis
4. Discussion of the results
5. Writing of the manuscript
6. Approval of the last version of the manuscript

H.E.R. has contributed to 1, 2, 3, 4, 5 and 6.

Acceptance Note: This article was approved by the journal editors Dr. Rafael Sotelo and Mag. Ing. Fernando A. Hernández Gobertti.